

PACS numbers: 42.55.Wd; 42.65.Ky; 42.70.Mp
DOI: 10.1070/QE2012v042n02ABEH014800

Frequency doubling of a tunable ytterbium-doped fibre laser in KTP crystals phase-matched in the *XY* and *YZ* planes

V.A. Akulov, S.I. Kablukov, S.A. Babin

Abstract. **This paper presents an experimental study of frequency doubling of a tunable ytterbium-doped fibre laser in KTP crystals phase-matched in the *XY* and *YZ* planes. In the *XY* plane, we obtained continuous tuning in the range 528–540 nm through intracavity frequency doubling. The second-harmonic power reached 450 mW for 18 W of multimode diode pump power, which was five times higher in comparison with single-pass frequency doubling. In a single-pass configuration in the *YZ* plane, we obtained a wide tuning range (527 – 551 nm) in the green spectral region and a second-harmonic power of ~10 mW. The tuning range was only limited by the mechanical performance of the fibre Bragg grating and can potentially be extended to the entire lasing range of the ytterbium-doped fibre laser.**

Keywords: *fibre lasers, frequency doubling, KTP, frequency tuning.*

1. Introduction

Ytterbium-doped fibre lasers with a relatively large gain bandwidth in the near-IR spectral region enable lasing between 1.03 and 1.15 μm (see e.g. Refs [1, 2]). Owing to this, the laser wavelength is rather easy to tune by compressing the fibre Bragg grating that serves as the cavity mirror of the fibre laser (see e.g. Refs [3, 4]).

Because of their simple design, high efficiency, high output beam quality and reliability, fibre lasers are an attractive alternative to other types of near-IR lasers. The advent of efficient visible light sources based on fibre lasers has considerably expanded their application field. Frequency doubling of ytterbium-doped fibre lasers enables conversion from the near IR to the visible range, with the possibility of wavelength tuning from the green (~515 nm) to yellow (~575 nm) spectral region. Many known lines of other laser sources fall in this range. Therefore, fibre lasers can be an alternative to conventional laser sources, e.g. to argon lasers operating at 515 nm and neodymium- or ytterbium-doped solid-state lasers emitting at 515, 532, 551 and 561 nm [5, 6]. In addition, the 'yellow-green' fibre lasers offer continuous wavelength tuning, which opens up new possibilities in applications that employ several lasers operating simultaneously at different fixed wavelengths (e.g. in flow cytometry [7]).

Despite all the advantages of fibre lasers, frequency doubling of tunable fibre lasers continues to be a challenge. In fibre laser harmonic generation, use is commonly made of single-pass configurations with expensive, periodically poled crystals. Using single-pass frequency doubling in a periodically poled crystal, Samanta et al. [8] obtained a second-harmonic power of 9.6 W at a 30-W fundamental harmonic input from a linearly polarised single-frequency ytterbium-doped fibre laser. In this approach, the tuning range (typically within 5 nm) is limited by the working temperature range of the crystal. High conversion efficiency can also be reached by external cavity frequency doubling (see e.g. Ref. [9]). This however requires a complex, expensive distributed feedback single-frequency fibre laser, which also has wavelength tuning limitations.

Cieslak and Clarkson [10] proposed yet another approach for efficient frequency doubling of fibre lasers. A fibre laser beam is directed to a four-mirror cavity containing a nonlinear crystal. The beam transmitted through the cavity is reflected back to the fibre by a high-reflectivity mirror placed behind the enhancement cavity, thereby providing feedback. The feedback enables the fibre laser to operate only on the eigenmodes of the four-mirror cavity, so that the fundamental mode power accumulates in the cavity, raising the frequency doubling efficiency. This configuration ensured a second-harmonic power of 19 W for 90 W of absorbed multimode pump power. The method enables frequency tuning in a wide range but relies on a rather complex experimental setup: a bulk diffraction grating is used instead of a fibre Bragg grating to select the fibre laser wavelength, and the configuration contains rather many optical components that require exact matching and tuning. Moreover, the second-harmonic spectrum contains several peaks due to longitudinal mode selection.

In many applications, including flow cytometry and confocal microscopy, high visible light powers are not needed: power levels of tens or hundreds of milliwatts are sufficient. It is therefore of great current interest to develop a simple fibre laser widely tunable in the visible range. Recent work [11] has demonstrated the possibility of efficient intracavity frequency doubling of fibre lasers. The frequency doubling of a tunable fibre laser in a KTP crystal with type II phase matching in the *XZ* plane was studied by Akulov et al. [12, 13]. They have demonstrated fibre laser wavelength tuning in the range 540–560 nm for single-pass frequency doubling in the KTP

V.A. Akulov Institute of Automation and Electrometry, Siberian Branch, Russian Academy of Sciences, prosp. Akad. Koptyuga 1, 630090 Novosibirsk, Russia; e-mail: akulov.v84@gmail.com;
S.I. Kablukov, S.A. Babin Institute of Automation and Electrometry, Siberian Branch, Russian Academy of Sciences, prosp. Akad. Koptyuga 1, 630090 Novosibirsk, Russia; Novosibirsk State University, ul. Pirogova 2, 630090 Novosibirsk, Russia; e-mail: kab@iae.nsk.su, babin@iae.nsk.su

Received 8 December 2011
Kvantovaya Elektronika **42** (2) 120–124 (2012)
Translated by O.M. Tsarev

crystal [12] and efficient intracavity frequency doubling with continuous wavelength tuning in the range 540–550 nm [13].

Since the phase matching condition in the *XZ* plane of KTP crystals is satisfied at wavelengths above 1080 nm, a crystal cut along other planes is needed to extend the second-harmonic generation range of KTP. This paper examines the possibility of frequency doubling of a tunable fibre laser in the *XY* and *YZ* planes of KTP crystals.

2. Experimental results

2.1. Frequency doubling in a KTP crystal in the *XY* plane

Frequency doubling in KTP crystals is known to require type II phase matching, which involves both the ordinary and extraordinary fundamental waves. Walk-off in a nonlinear crystal reduces the second-harmonic generation efficiency. The most efficient second-harmonic generation occurs where the ordinary and extraordinary beams overlap. For efficient conversion, walk-off should be reduced. A walk-off compensation technique for fundamental waves was proposed by Asaumi [14]. To compensate the walk-off of the extraordinary fundamental wave and improve the conversion efficiency, an obliquely incident beam was used. By selecting an appropriate crystal geometry, one can reduce the walk-off and, hence, optimise second-harmonic conversion at a necessary wavelength. As shown by Asaumi [14], at $\lambda = 1064$ nm the walk-off in a KTP crystal whose crystallographic axis *X* makes an angle $\varphi = 29°$ with the normal to the crystal surface is compensated for at an angle of incidence of 7°. In this geometry, the second-harmonic generation efficiency is more than 20% above that at normal incidence ($\varphi = 24.5°$).

In this study, frequency doubling has been achieved using a KTP crystal with type II phase matching in the *XY* plane and $\varphi = 21°$. The geometrical length of the optical path in the crystal at 1070 nm is 8 mm. The geometry chosen enables the walk-off between the ordinary and extraordinary fundamental beams at 1070 nm to be compensated for at an angle of incidence of 5.5°. Figure 1 shows the calculated angle of incidence and walk-off angle as functions of phase matching wavelength.

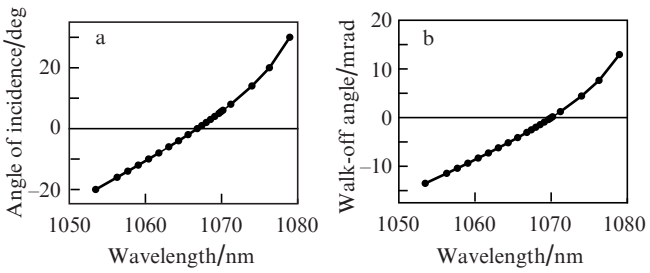

Figure 1. (a) Angle of incidence on a KTP crystal (*XY* plane) and (b) angle between the fundamental beams as functions of phase matching wavelength.

Zero walk-off angle corresponds to the optimal second-harmonic generation coefficient because the ordinary and extraordinary beams then coincide (Fig. 1b). A deviation from zero angle reduces the conversion coefficient, but there is an angular range where it differs only slightly from the maximum value. The spectral range where the crystal is capable of efficient frequency doubling is thus rather easy to find [12]. In particular, it follows from Fig. 1b that the angle between the ordinary and extraordinary fundamental beams is within 10 mrad at $\lambda = 1058–1077$ nm, which may point to a relatively high second-harmonic generation efficiency in this range.

The experimental setup used (Fig. 2) was similar to that described previously [13]. The pump beams from 976-nm multimode diode lasers (*2*) were coupled into a double-clad ytterbium-doped active fibre (*4*) through a pump coupler (*3*) having six multimode input ports and one single-mode input port, with a tunable fibre Bragg grating (*1*) fusion-spliced to it. The IR beam at the fundamental frequency was collimated by a lens (*5*), reflected by a selective scanning mirror (*6*) and focused by another lens (*7*) into a nonlinear crystal (*8*). The crystal was placed in a thermostat whose temperature was maintained by a controller (*9*).

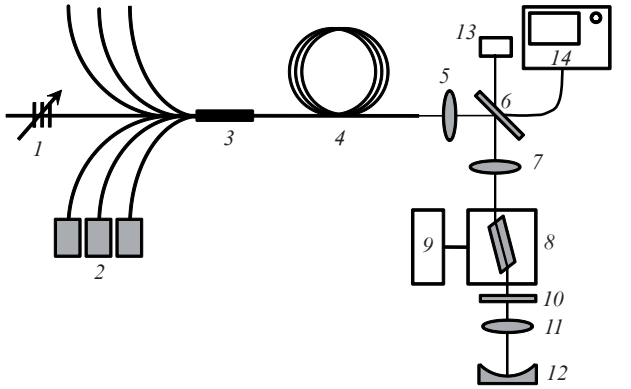

Figure 2. Schematic of the experimental setup (see text for designations).

The laser cavity was formed by an output mirror (*12*) and the grating (*1*). The mirror (*12*) had high reflectivity at both the fundamental and second-harmonic frequencies. The second-harmonic radiation generated in the crystal on two passes was decoupled from the cavity by the selective mirror (*6*) and detected by a power meter (*13*). The wavelength was measured by an optical spectrum analyser (*14*). Like in a previous study [13], an extra optical element (*10*), intended for phase compensation, was placed between the crystal (*8*) and the lens (*11*) of the output mirror.

Our experiments were performed as follows: the fibre laser wavelength was varied using the tunable fibre Bragg grating, and at each wavelength the second-harmonic power was maximised by rotating the crystal. Figure 3 shows the second-harmonic power as a function of wavelength for intracavity and single-pass frequency doubling. In the latter case, the maximum second-harmonic power was 90 mW at $\lambda = 535.5$ nm and a multimode diode pump power of 18 W. Comparison of the experimental data in Fig. 3 with the walk-off angle calculation results in Fig. 1b leads us to conclude that the tuning range (528–540 nm) fits well with the above estimate of the walk-off angle (within 10 mrad). This approach is much simpler than calculation of the conversion coefficient as a function of wavelength for a particular crystal geometry, which requires finding rather complicated integrals.

It follows from Fig. 1a that normal incidence corresponds to $\lambda = 1067$ nm (533.5 nm). The angle between the fundamen-

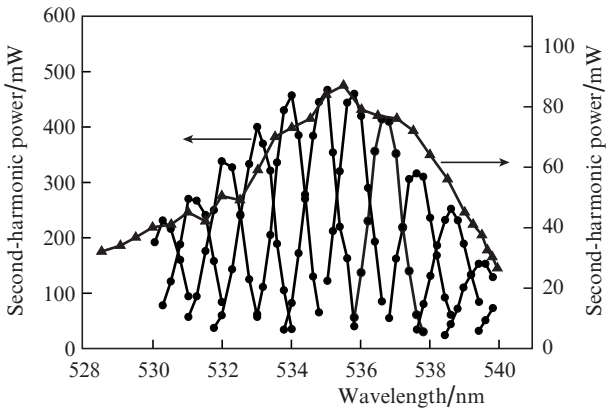

Figure 3. Second-harmonic power as a function of wavelength for intracavity (●) and single-pass (▲) frequency doubling.

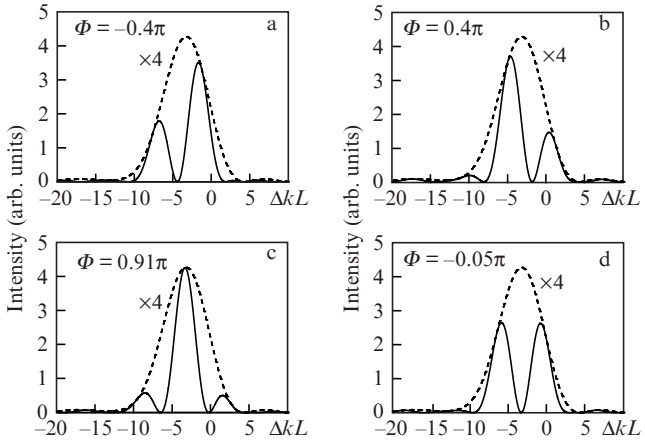

Figure 4. Phase matching curves for a double-pass (solid lines) and a single-pass (dashed lines) second-harmonic generation at different phases (Φ).

tal beams is then 5 mrad (Fig. 1b). At the above wavelength, the second-harmonic power for single-pass frequency doubling was 70 mW. Thus, an increase in the angle between the fundamental beams from 0 to 5 mrad reduced the second-harmonic power by 20%.

In the case of intracavity frequency doubling, the spectral dependence of the second-harmonic power differs from that for single-pass frequency doubling because the cavity contains optical elements with significant dispersion (a lens and others) behind the crystal, which produce a phase shift between the fundamental and second harmonics on the forward and backward passes. This leads to interference of the second-harmonic beams generated on these passes. The interference, in turn, modifies the phase matching curve, which can be represented in the case of single-pass frequency doubling by $(\sin x/x)^2$, where x is proportional to the wave vector mismatch. This effect was qualitatively interpreted previously [13]. From a system of reduced equations for a cylindrically symmetric Gaussian beam with no walk-off, the following expression for the second-harmonic power was derived:

$$P_2 \propto \left| \int_0^L \left\{ \frac{\exp(i\Delta k z')}{1 - i2(z' - z_0)/b} + \exp(i\Phi + i\Delta k L) \frac{\exp(i\Delta k z')}{1 - i2[(z' - (L - z_0)]/b} \right\} dz' \right|^2, \quad (1)$$

where $\Delta k = K - 2k$ is the wave vector mismatch; k and K are the wave vectors of the fundamental and second harmonics, respectively; L is the crystal length; $b = kw_0^2$ is the confocal parameter; w_0 is the waist radius; z_0 is the distance from the input face of the crystal to the waist; $\Phi = \varphi_2 - 2\varphi_1$; and φ_1 and φ_2 are the phases of the fundamental and second harmonics, respectively.

It can be verified that, like in the well-known case of second-harmonic generation optimisation for a Gaussian beam in the single-pass configuration described by Boyd and Kleinman [15], an optimum is reached when the beam is focused into the centre of the crystal ($z_0 = L/2$, $b = L/2.84$). Figure 4 shows the phase matching curves obtained for a double-pass configuration at different phases (Φ) by numerically calculating integral (1) with optimal b and z_0. As seen, there is an optimal phase which ensures the highest second-harmonic power (Fig. 4c). To achieve this at all lasing wavelengths, one should optimise the phase, thereby reaching the highest second-harmonic power.

To this end, an extra optical element that allowed the phase to be varied was placed between the crystal and the lens (*11*) (Fig. 2). After each wavelength change with the use of this element, the phase was optimised so as to maximise the second-harmonic power. Figure 5 presents two experimental phase matching curves for a compensated and an uncompensated phase. The curves were obtained as follows: At a particular wavelength, the crystal was adjusted to the phase matching angle and then the phase Φ was varied to maximise [curve (*1*)] or minimise [curve (*2*)] the second-harmonic power. Next, varying the centre wavelength of the Bragg grating, we measured the second-harmonic power as a function of wavelength. The crystal was adjusted at $\lambda = 535.04$ nm for curve (*1*) and at $\lambda = 535.16$ nm for curve (*2*), so the curves are displaced relative to one another. It can be seen that, at any lasing wavelength, one can reach phase compensation, thereby maximising the conversion efficiency.

In this way, using phase compensation we obtained a relatively smooth spectral dependence of the second-harmonic

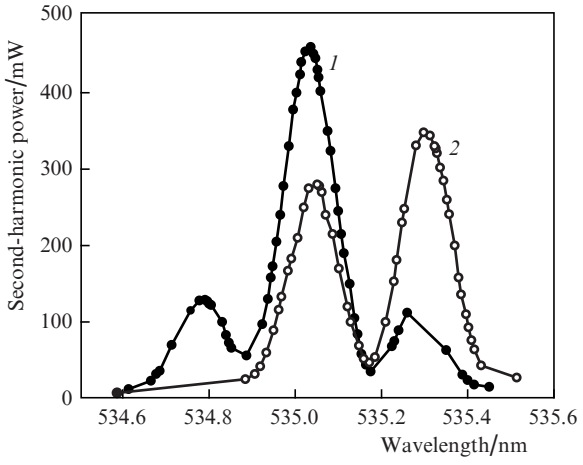

Figure 5. Experimental phase matching curves for (*1*) a compensated and (*2*) an uncompensated phase.

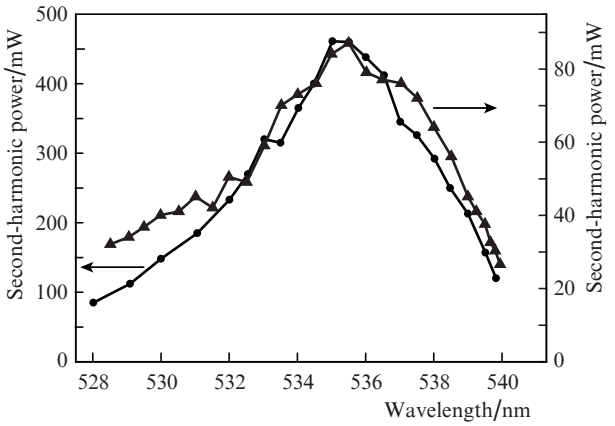

Figure 6. Tuning curves for intracavity (●) and single-pass (▲) frequency doubling.

power (Fig. 6), similar in shape to that for single-pass frequency doubling, but with a power higher by about a factor of 5. The tuning range was 12 nm wide (528–540 nm). The second-harmonic output power reached 450 mW for 18 W of multimode diode pump power.

2.2. Frequency doubling in a KTP crystal in the *YZ* plane

The nonlinearity coefficient of KTP crystals in the *YZ* plane is smaller than that in the *XY* plane: $d_{\text{eff}}^{YZ} \approx 0.5 d_{\text{eff}}^{XY}$. At a wavelength of 1070 nm, the walk-off angle of an extraordinary fundamental wave is 2.6 mrad in the *XY* plane and 34 mrad in the *YZ* plane. A large walk-off considerably reduces the second-harmonic generation efficiency because, in contrast to type I phase matching, in the case of type II phase matching the generation process involves both the ordinary and extraordinary fundamental beams, and the walk-off between the beams reduces the overlap region, where energy is transferred to the second harmonic [16]. An important feature of the *YZ* plane of KTP crystals is that the phase matching condition is satisfied here over the entire lasing range of the ytterbium-doped fibre laser. In view of this, to obtain a complete picture of the process, we examine frequency doubling of a widely tunable fibre laser in a KTP crystal phase-matched in the *YZ* plane, whose crystallographic axis *Z* makes an angle $\theta = 88°$ with the normal to the crystal surface. Like above, the geometrical length of the optical path in the crystal at 1070 nm is 8 mm.

For the crystal geometry chosen, we calculated the angle of incidence and angle between the fundamental beams as functions of wavelength (Fig. 7). As seen in Fig. 7b, complete walk-off compensation (zero walk-off angle) takes place at a wavelength of ~1000 nm, which falls beyond the lasing range of the ytterbium-doped fibre laser. It can be shown that complete walk-off compensation is possible in the range 1000–1053 nm, but at 1053 nm it can only be reached at grazing incidence. Because of this, the crystal geometry was chosen so as to partially compensate the walk-off in the lasing range of the ytterbium-doped fibre laser while keeping the angle of incidence not very large. Considerable angles of incidence have a significant effect on the surface transmittance. In the crystal geometry in question, the angle between the fundamental beams at 1070 nm is 13.4 mrad. As mentioned above, at normal incidence the angle between the fundamental beams in a KTP crystal phase-matched in the *YZ* plane is

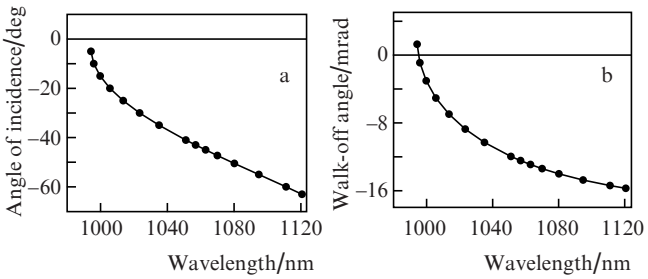

Figure 7. (a) Angle of incidence on a KTP crystal (*YZ* plane) and (b) angle between the fundamental beams as functions of phase matching wavelength.

34 mrad. Thus, using an obliquely incident beam, we were able to compensate the walk-off by more than 20 mrad.

Figure 8 shows the spectral dependence of the second-harmonic conversion coefficient [the ratio of the second-harmonic power, P_2, to the square of the fundamental (IR) harmonic power, P_1] for single-pass frequency doubling. The output power of the ytterbium-doped fibre laser was 13 W. The conversion coefficient is seen to increase with decreasing walk-off angle between the beams. The second-harmonic power was 2.5–9 mW for 18 W of multimode diode pump power. This is an order of magnitude lower in comparison with the crystal phase-matched in the *XY* plane (Fig. 6), which offered a maximum power of 90 mW at the same pump power.

In the case of intracavity frequency doubling, the second-harmonic power at 1102 nm was 12.1 mW, which is almost a factor of 5 higher than that for single-pass frequency doubling. The key distinction of the *YZ* plane from the other two planes of KTP crystals is that it offers a wide tuning range, which covers the entire lasing range of the ytterbium-doped fibre laser (1030 to 1120 nm). In our experiments, we achieved tuning over 24 nm (527–551 nm) in the visible range. Given that the walk-off angle decreases with decreasing wavelength, even higher efficiency can be reached with this KTP at 515 nm. The main limitation for wavelength tuning is the damage threshold of the fibre in which the Bragg grating is inscribed. In the case of axial compression, the wavelength tuning range in the IR is about 7% around the initial resonance wavelength of the grating [17].

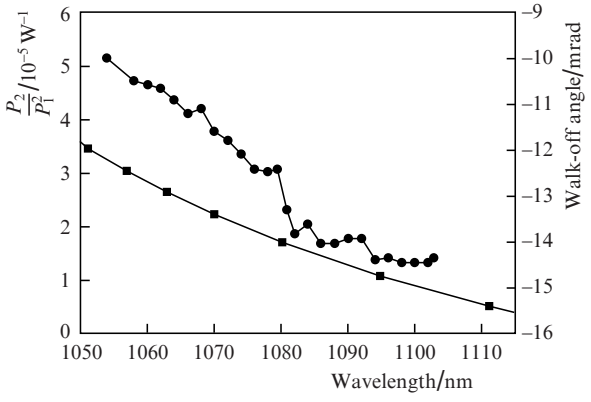

Figure 8. Spectral dependences of the second-harmonic conversion coefficient (●) and walk-off angle between the fundamental beams (■).

3. Conclusions

We have studied frequency doubling of a tunable fibre laser in KTP crystals phase-matched in two different planes. In the *XY* plane, we obtained continuous tuning in the range 528 – 540 nm through intracavity frequency doubling. The continuous tuning was due to an additional phase shift element in the laser cavity. Adjusting this element ensured the maximum second-harmonic conversion efficiency at each wavelength owing to the tuning of the relative phase between the second and fundamental harmonics. The highest output power at 535 nm was 450 mW for 18 W of multimode diode pump power. In single-pass frequency doubling, the highest power was 90 mW at the same pump power. Thus, intracavity frequency doubling was five times as efficient as the single-pass configuration.

In the *YZ* plane of a KTP crystal in a single-pass configuration, we obtained a wider tuning range (527 – 551 nm, i.e. 24 nm in the green spectral region), which was only limited by the mechanical performance of the fibre Bragg grating and can be extended to the entire lasing range of the ytterbium-doped fibre laser (1030 – 1120 nm). Using an obliquely incident beam, we were able to compensate the walk-off between the fundamental beams by 20 mrad, but we failed to achieve complete walk-off compensation over the entire lasing range of the ytterbium-doped fibre laser because large angles of incidence had to be used. The conversion efficiency was then an order of magnitude lower in comparison with the other planes of KTP crystals. The second-harmonic power was 2.5 – 9 mW for 18 W of multimode diode pump power. In intracavity frequency doubling in this plane, we were also able to increase the second-harmonic power by five times, which was checked only at one wavelength (551 nm). The two proposed tunable 'green' fibre lasers (one with a relatively high power and the other with a wide tuning range) can find application, in particular in flow cytometry [7].

References

1. Kurkov A.S., Dianov E.M. *Kvantovaya Elektron*., **34**, 881 (2004) [*Quantum Electron*., **34**, 881 (2004)].
2. Harun S.W., Moghaddam M.R.A., Dimyati K., Ahmad H. *Laser Phys. Lett*., **6**, 458 (2009).
3. Abdulina S.R., Babin S..A., Vlasov A.A., Kablukov S.I., Kurkov A.S., Shelemba I.S. *Kvantovaya Elektron*., **37**, 1146 (2007) [*Quantum Electron.*, **37**, 1146 (2007)].
4. Peterka P., Maria J., Dussardier B., Slavik R., Honzátko P., Kubeček V. *Laser Phys. Lett*., **6**, 732 (2009).
5. Weber M.J. *Handbook of Lasers* (Berkeley, California: CRC Press, 2001).
6. Webb C.E., Jones J.D.C. *Handbook of Laser Technology and Applications* (Bristol, Philadelphia, Institute of Physics, 2004).
7. Telford W.G., Babin S.A., Khorev S.V., Rowe S.H. *Cytometry A*, **75**, 1031 (2009).
8. Samanta G.K., Chaitanya Kumar S., Ebrahim-Zadeh M. *Opt. Lett*., **34**, 1561 (2009).
9. Markert F., Scheid M., Kolbe D., Walz J. *Opt. Express*, **15**, 14476 (2007).
10. Cieslak R., Clarkson W.A. *Opt. Lett*., **36**, 1896 (2011).
11. Akulov V.A., Afanasiev D.M., Babin S.A., Churkin D.V., Kablukov S.I., Rybakov M.A., Vlasov A.A. *Laser Phys.,* **17***,* 124 (2007).
12. Akulov V.A., Babin S.A., Kablukov S.I., Vlasov A.A. *Laser Phys*., **18**, 1225 (2008).
13. Akulov V.A., Babin S.A., Kablukov S.I., Raspopin K.S. *Laser Phys*., **21**, 935 (2011).
14. Katsu Asaumi. *Appl. Opt*., **37**, 555 (1998).
15. Boyd G.D., Kleinman D.A. *J. Appl. Phys*., **39**, 3597 (1968).
16. Zondy J.-J. *Opt. Commun*., **81**, 427 (1991).
17. Mokhtar M.R., Goh C.S., Butler S.A., et al. *Electron. Lett.,* **39**, 509 (2003).